Neutron-Scattering Studies Reveal Further Details of the Ca^{2+}/Calmodulin-Dependent Activation Mechanism of Myosin Light Chain Kinase†

Joanna K. Krueger,‡ Gang Zhi,§ James T. Stull,§ and Jill Trewhella*,‡

Chemical Science and Technology Division, Mail Stop G758, Los Alamos National Laboratory, Los Alamos, New Mexico 87545, and Physiology Department, University of Texas Southwestern Medical Center at Dallas, Dallas, Texas 75235-9040

Received June 2, 1998

ABSTRACT: Previously, we utilized small-angle X-ray scattering and neutron scattering with contrast variation to obtain the first low-resolution structure of $4Ca^{2+}$·calmodulin (CaM) complexed with a functional enzyme, an enzymatically active truncation mutant of skeletal muscle myosin light chain kinase (MLCK). These experiments showed that, upon binding to MLCK, CaM undergoes a conformational collapse identical to that observed when CaM binds to the isolated peptide corresponding to the CaM binding sequence of MLCK. CaM thereby was shown to release the inhibition of the kinase by inducing a significant movement of its CaM binding and autoinhibitory sequences away from the surface of the catalytic core [Krueger, J. K., Olah, G. A., Rokop, S. E., Zhi, G., Stull, J. T., and Trewhella, J. (1997) *Biochemistry 36*, 6017−6023]. We report here similar scattering experiments on the CaM·MLCK complex with the addition of substrates; a nonhydrolyzable analogue of adenosine-triphosphate, AMPPNP, and a peptide substrate for MLCK, a phosphorylation sequence from myosin regulatory light chain (pRLC). These substrates are shown to induce an overall compaction of the complex. The separation of the centers-of-mass of the CaM and MLCK components is shortened (by ∼12 Å), thus bringing CaM closer to the catalytic site compared to the complex without substrates. In addition, there appears to be a reorientation of CaM with respect to the kinase upon substrate binding that results in interactions between the N-terminal sequence of CaM and the kinase that were not observed in the complex without substrates. Finally, the kinase itself becomes more compact in the CaM·MLCK·pRLC·AMPPNP complex compared to the complex without substrates. This observed compaction of MLCK upon substrate binding is similar to that arising from the closure of the catalytic cleft in cAMP-dependent protein kinase upon binding pseudosubstrate.

Calmodulin is the major intracellular receptor for Ca^{2+} and is responsible for the Ca^{2+}-dependent regulation of a wide variety of cellular processes via interactions with a diverse array of target enzymes including a number of kinases. The Ca^{2+}/calmodulin (CaM)-dependent activation of myosin light chain kinase (MLCK) is a model for CaM-kinase interactions that has been investigated extensively. In its activated form, MLCK catalyzes the transfer of the terminal phosphoryl group from a bound adenosine-triphosphate moiety to the hydroxyl group of a serine located near the N-terminus of the myosin regulatory light chain. This phosphorylation event results in the potentiation of skeletal muscle contraction (*2*), plays important roles in nonmuscle processes such as endothelial cell retraction, secretion, platelet aggregation, and exocytosis, and is essential for smooth muscle contraction (*3*). All isoforms of MLCK include a conserved catalytic core homologous to that of other protein kinases, followed immediately by a carboxyl-terminal regulatory segment consisting of both an auto-inhibitory sequence and a CaM-binding sequence (*4*, *5*). In its inhibited conformation, the regulatory segment of MLCK maintains numerous contacts with the catalytic core, thus preventing substrate binding (*6*−*8*). CaM has an unusual dumbbell-shaped structure with two globular lobes connected by an extended helix, each having two Ca^{2+}-binding EF-hand motifs (*9*). When Ca^{2+} binds to calmodulin, hydrophobic clefts on each globular lobe that are important in target enzyme recognition and binding are exposed (reviewed in refs *10* and *11*). Small-angle X-ray and neutron scattering (*12*), NMR (*13*), and X-ray crystallography (*14*) of complexes of CaM with isolated peptides based on CaM-binding sequences from smooth and skeletal muscle MLCKs demonstrate that CaM undergoes a dramatic conformational collapse upon binding these peptides. The collapse is achieved via the flexibility in the interconnecting helix region, which allows the two lobes of the dumbbell-shaped CaM to come into close contact, encompassing the peptide as the hydrophobic clefts in the globular lobes of CaM interact with hydrophobic residues in the helical target peptide. Recently, we obtained a structural model of CaM complexed with a catalytically competent truncation mutant

† This work was performed under the auspices of the Department of Energy under contract to the University of California, supported by DOE project KP-11-01-01-0 (J.T.), and NIH Grants GM40528 (J.T.), HL06296 (J.T.S.), and HL26043 (J.T.S.). Neutron-scattering data were obtained using instrumentation supported by NSF under Agreement DMR-9423101 at the Cold Neutron Research Facility at the National Institute of Standards Technology. X-ray-scattering data were obtained at the Stanford Synchrotron Research Laboratory using instrumentation supported by the DOE (Basic Energy Sciences and Office of Health and Environmental Research) and the NIH Biomedical Resource Technology Program, Division of Research Resources.

* Author to whom correspondence should be addressed.

‡ Los Alamos National Laboratory.

§ University of Texas Southwestern Medical Center at Dallas.

S0006-2960(98)01311-7 CCC: $15.00
Published on Web 09/15/1998

of MLCK (*1*) using small-angle neutron scattering with contrast variation. The truncated kinase contains the catalytic domain and regulatory segment and shows similar catalytic and activation properties compared to the full-length MLCK (*15*). Our scattering data show that upon binding MLCK, CaM achieves a final collapsed conformation identical to that observed for CaM when bound to the isolated CaM-binding peptide sequence from MLCK. This experiment provided direct structural evidence that CaM releases the kinase inhibition by inducing a significant movement of the CaM binding and autoinhibitory sequences away from the surface of the catalytic core.

To study the structural effects of substrate binding to the CaM·MLCK complex, we have completed small-angle X-ray and neutron scattering studies on a complex of deuterated CaM and the truncated skeletal MLCK in the presence of a nonhydrolyzable analogue of adenosine-triphosphate, AMPPNP, and the phosphorylatable sequence of the myosin regulatory light chain, pRLC. Small-angle scattering gives information on the overall shapes of proteins in solution. Because of the different neutron-scattering properties of deuterium and hydrogen, deuterium labeling facilitates extraction of structural information on the individual components of the complex using contrast variation techniques. Thus, the experiments described here provide a low-resolution structural model of the CaM·MLCK·pRLC·AMPPNP complex, including information of the conformations of the individual components. These data are compared to the previous scattering data on CaM·MLCK in the absence of substrates (*1*) to evaluate the changes that occur within the complex upon substrate binding to MLCK.

MATERIALS AND METHODS

Protein Sample Preparation. MLCK (residues 257−607 of the skeletal muscle form) was purified as described by Gao et al. (*15*) with the addition of an FPLC gel filtration (S12, Pharmacia) step. Column elution buffer contained 20 mM 3-(*N*-morpholino)propanesulfonic acid (MOPS), pH 8.0, 25 mM KCl, 5 mM magnesium acetate, 0.2 mM $CaCl_2$, 1 mM dithiothreitol (DTT), and 2.5% glycerol. Calmodulin, in both deuterated (dCaM) and nondeuterated (hCaM) forms, was prepared as described in Heidorn et al. (*12*) followed by extensive dialysis against the identical buffer that was used for the kinase's final FPLC elution buffer. Samples of the complex were prepared with partially deuterated CaM in which 62% of the nonexchangeable hydrogen atoms was substituted with deuterium (62dCaM). Partial deuteration was achieved as described for troponin C (*16*). The level of deuteration was determined using NMR by comparing total NMR intensity for hCaM versus dCaM from samples of known concentrations. The deuteration level was checked by plotting the square root of the experimentally determined forward scatter, $I(0)$, versus the percent solvent deuteration for each contrast point measured in the neutron-scattering experiments. The *x*-intercept gives the percent solvent deuteration at zero contrast. At this value, the average scattering density for the complex, ρ_{ave}, equals that of the solvent, ρ_s. The value of ρ_{ave} can be calculated from the chemical and isotopic composition of CaM and MLCK. Since the isotopic composition of CaM is the only unknown it can be determined by equating ρ_{ave} with ρ_s, assuming a partial specific volume of 0.72 cm^3/g and that 45% of all labile hydrogens exchange (*16*).

CaM·MLCK·pRLC·MPPNP Complex Formation. All complexes were formed by mixing the components immediately prior to scattering data collection in order to avoid nonspecific aggregation. The myosin regulatory light chain peptide, pRLC, used in these studies was synthesized with the sequence KKRAARATSNVFS (*17*), brought up in 10 mM MOPS/1mM EDTA, and the final peptide concentration of which was determined by amino acid analysis. AMPPNP (Sigma Product no. A2647) was stored at −70 °C and made up fresh in FPLC buffer just prior to experimentation. Because of the low extinction coefficient for CaM, the concentration determination for the 62dCaM sample was checked by measuring the small-angle scattering and analyzing the forward scattering which, for monodisperse protein samples, is linearly dependent on the protein concentration (*18*). Concentrations of MLCK were determined spectrophotometrically using an extinction coefficient of 0.91 L/g cm at 280 nm. For the neutron contrast series on the complex, samples were prepared as 62dCaM:MLCK:pRLC:AMPPNP with stoichiometries of 1:1:1.5:1.5 and total protein concentrations of 2.0, 2.0, 0.70, 0.65, and 0.40 mg/mL in solutions containing 0, 20, 40, 75, and 85% D_2O, respectively. Samples for X-ray-scattering experiments were prepared similarly to those for the neutron experiment in H_2O. Samples for the 82% D_2O 62dCaM solvent matching neutron experiments were prepared as mixtures of 62dCaM:MLCK:pRLC:AMPPNP, 62dCaM:MLCK:pRLC, and 62dCaM:MLCK:AMPPNP with stoichiometries of 1:1:1.5:1.5, 1:1:1.5 and 1:1:1.5 and final total protein concentrations of 0.39, 0.42, and 0.45 mg/mL, respectively.

Scattering Data Acquisition. X-ray-scattering data were collected using beam line 4−2 at the Stanford Synchrotron Radiation Line (SSRL) (*19*), as well as the X-ray instrument at Los Alamos described in Heidorn and Trewhella (*20*). X-ray data shown here are those from SSRL since the high-intensity synchrotron source gave dramatically increased statistical precision. Comparison of the synchrotron data with data measured on the same sample preparations at Los Alamos using the much weaker sealed tube source showed that radiation damage effects due to the high X-ray intensities at the synchrotron were minimal. All neutron-scattering measurements were performed with the 30 m SANS instrument (NG3) at the National Institute of Standards and Technology (NIST) (*21*). Neutrons with a mean wavelength of 5.0 Å were used with a full-width-at-half-maximum (fwhm) of 34%. For the 0, 20, 75, 82, and 85% D_2O samples, sample-to-detector distances utilized were 6 and 1.5 m to give data over the Q range 0.015−0.37 $Å^{-1}$. The excellent overlap of the 6 and 1.5 m data in the Q range 0.048−0.077 Å was used to scale these two data sets relative to each other. Data for the 82% D_2O 62dCaM solvent matching experiment were collected using an independent sample preparation. Data for the 40% D_2O sample were collected using a third independent sample preparation and a 2.1 m sample-to-detector distance (Q range 0.035−0.28 $Å^{-1}$). Sample cells were 1-mm path-length quartz cuvettes for 0, 20, and 40% D_2O, and 4-mm path-length quartz cuvettes for 75, 82, and 85% D_2O (since neutron transmissions are higher for these samples due to their lower H content).

Scattering Data Analysis. The scattering of neutrons (or X-rays) from a homogeneous solution of monodisperse particles (such as proteins or protein complexes) can be expressed as

$$I(Q) = \langle \int |[\rho(\mathbf{r}) - \rho_s]\exp[-i(\mathbf{Q}\cdot\mathbf{r})\, d\mathbf{r}]|^2 \rangle \qquad (1)$$

where $Q = 4\pi(\sin\theta)/\lambda$ is the amplitude of the scattering vector (2θ is the scattering angle and λ is the wavelength of the X-rays or neutrons), $\rho(\mathbf{r})$ and ρ_s are the scattering densities for the protein and solvent, respectively, the integration is taken over the volume of the particle, and the broken brackets ($\langle\rangle$) denote the average over all particle orientations. The scattering data were analyzed as previously described (*12*, *16*). In the case of neutrons, one can take advantage of the large difference in neutron scattering lengths between hydrogen and deuterium. By deuterating one component of a complex and using "contrast variation" (*22*, *23*) one can obtain information on the conformations and dispositions of the individual components in the complex. Assuming internal scattering density fluctuations are negligible, the total scattering from a complex of a deuterated and nondeuterated protein can be written as

$$I(Q,\Delta\rho_C,\Delta\rho_K) = \Delta\rho_C{}^2 I_C(Q) + \Delta\rho_C\Delta\rho_K I_{CK}(Q) + \Delta\rho_K{}^2 I_K(Q) \qquad (2)$$

where the subscripts C and K refer to dCaM and MLCK, respectively. $\Delta\rho_C$ equals $\rho_C - \rho_S$ where ρ_C is the mean scattering density for dCaM. A similar definition holds for $\Delta\rho_K$. The three basic scattering functions in eq 2 are $I_C(Q)$ and $I_K(Q)$, representing the scattering due to the individual components in the complex, and $I_{CK}(Q)$ which is the cross-term. The inverse Fourier transform of $I(Q)$ yields $P(r)$, the probable frequency distribution of interatomic vectors within the scattering particle. $P(r)$ goes to zero at the maximum linear dimension, d_{max}, of the scattering particle and its zeroth and second moments give the forward scatter, I_0, and radius of gyration, R_g, respectively.

Modeling the Scattering Data. The scattering data were modeled using a uniform-density, two-ellipsoid model for the complex and a Monte Carlo simulation program SASMODEL (*24*). The program determines the shapes and relative dispositions of macromolecular components (domains or subunits) by testing large numbers of models against scattering data. Each molecular component is described as a low-resolution object, such as an ellipsoid. In this study, the basic scattering functions for CaM and MLCK were used to find best-fit one-ellipsoid models for each individual component of the complex. The average values of the ellipsoid axis lengths ($\pm 10-20\%$) were then used as constraints in a two-ellipsoid model search against all of the scattering data. During this model search, the position and orientation parameters of each ellipsoid to be optimized were generated by a random search. The two ellipsoids were constrained to have surface contact with each other. To test each model against the scattering data, a rapid Monte Carlo integration method (*20*) is used to generate model $P(r)$ functions. The objects defining a model are filled with random points and $P(r)$ is calculated by summing all pairwise combinations of these points. The corresponding $I(Q)$ is calculated by Fourier transformation of $P(r)$ and compared with the experimental data by means of least-squares methods. The points defining the models having the best least-squares deviations from the experimental data are saved in Brookhaven Protein Data Bank (PDB) format for easy viewing.

Evaluation of Samples for Aggregation. Extraction of structural information on individual proteins or protein complexes in solution from scattering data requires samples that are rigorously aggregation free. The zero angle or forward scattering, I_0, when normalized to the protein concentration in milligrams per milliliter, is directly proportional to the molecular weight of the scattering particle and, hence, is extremely sensitive to aggregation (*18*). I_0 values derived from X-ray scattering data of CaM·MLCK·pRLC·AMPPNP preparations were compared with those of a standard protein [lysozyme (*18*) or CaM (*20*)] known to be monodisperse and measured in the same sample cell on the same day. All scattering data used for structural analysis were taken from samples that were determined to be aggregation free based on analysis of I_0 values. Molecular volumes, V, were also calculated from the small-angle X-ray scattering data and from the basic scattering functions derived from the neutron scattering data using the relationship $V = 2\pi^2 I_0/Q_i$ where Q_i is the scattering invariant (*25*). The volumes thus derived (Table 1) were all within experimental error of the values calculated using the protein's molecular weight and the specific volume for a typical protein of 0.72 cm^3/g, confirming that our samples were aggregation-free for the duration of the scattering experiments. The CaM·MLCK·pRLC·AMPPNP complex did not show the nonspecific aggregation that we consistently observed within a few hours for CaM·MLCK samples in the absence of substrates (*1*).

RESULTS AND DISCUSSION

Small-Angle X-ray Scattering Results for the Overall Complex. The $P(r)$ function calculated from the X-ray-scattering data for CaM·MLCK·pRLC·AMPPNP is compared with that for CaM·MLCK in Figure 1, and Table 1 gives the respective structural parameters. The $P(r)$ function for the complex with substrates bound indicates a somewhat more compact, globular structure compared to that without substrates. The peak in the $P(r)$ profile of the complex with substrates is at a longer r value ($\sim$31 Å compared to $\sim$27 Å), but d_{max} is smaller (by 18 Å) as is R_g (by 2.4 Å). In addition, the shoulder at 55 Å seen in the $P(r)$ for the complex without substrates is less pronounced in the $P(r)$ for the complex with substrates. These data indicate an overall compaction of the structure upon substrate binding consistent with a movement of the centers of mass of the globular CaM and MLCK components toward each other.

Extraction of the Basic Scattering Functions from the Contrast Series Data. Each neutron-scattering measurement at a given D_2O concentration gives an equation in the form of eq 2 ("contrast points"). An additional equation is obtained from the X-ray-scattering data that has been appropriately scaled to the neutron-scattering data (eq 24.8 in ref *26*). Neutron-scattering data from CaM·MLCK·pRLC·AMPPNP at the five measured D_2O:H_2O ratios, as well as the corresponding X-ray scattering data, are shown in Figure 2A. A multiple linear regression routine was used to solve

Table 1: Structural Parameters of CaM·MLCK and Its Individual Components with and without MLCK Substrates[a]

	R_g (Å)	d_{max} (Å)	volume (Å^3)
from X-ray-scattering data			
CaM·MLCK·pRLC·AMPPNP	31.6 ± 1.2	100 ± 5	89 000 ± 11400
CaM·MLCK (*1*)	34.0 ± 0.7	118 ± 4	79 200 ± 5300
MLCK	25.8 ± 0.6	95 ± 10	68 580 ± 2200
cAPK plus PKI(5−22)amide (*28*)	21.0 ± 0.4	62 ± 3	52 275 ± 6325
cAPK (*28*)	23.0 ± 0.4	73 ± 3	52 980 ± 2790
from the basic scattering functions			
MLCK (plus substrates)	21.9 ± 0.5	68 ± 5	37 060 ± 2720
MLCK (minus substrates) (*1*)	24.6 ± 0.6	78 ± 4	49 750 ± 4230
CaM (plus MLCK substrates)	18.1 ± 1.5	53 ± 6	24 000 ± 5000
CaM (minus MLCK substrates) (*1*)	17.3 ± 0.4	49 ± 3	27 000 ± 3750

[a] Errors in the reported values for radius of gyration, R_g, and volume reflect only the counting statistics. Errors in d_{max} values reflect the confidence with which they are determined from each $P(r)$ function.

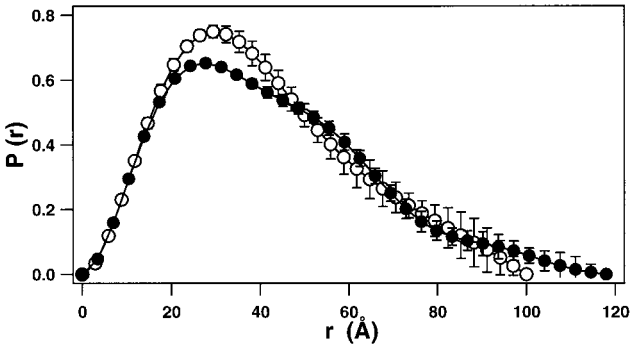

FIGURE 1: $P(r)$ functions, scaled by their respective molecular weights, for CaM·MLCK·pRLC·AMPPNP (○) and for CaM·MLCK (●) derived from the small-angle X-ray scattering data.

the linear equations for the three basic scattering functions $I_C(Q)$, $I_K(Q)$, and $I_{CK}(Q)$ (Figure 2B). Corresponding $P(r)$ functions for the individual components, MLCK·pRLC·AMPPNP and CaM (Figure 3), could then be calculated as the inverse Fourier transform of their respective $I(Q)$ vs Q profiles (*27*).

The $P(r)$ function for CaM within the CaM·MLCK·pRLC·AMPPNP complex derived from the basic scattering function $I_C(Q)$ shows that the bound CaM has a compact, globular structure that is the same (within error) as that of CaM within the CaM·MLCK complex without substrates present (Figure 3A). Therefore, the changes observed for the structure of the overall complex must come from changes in the MLCK·pRLC·AMPPNP component and/or the relative disposition of the two components. $P(r)$ for unactivated MLCK calculated from X-ray scattering data (Figure 3B) shows a peak at ∼30 Å, consistent with a globular prolate ellipsoid shape with dimensions somewhat larger than the catalytic core of the related cAMP-dependent protein kinase, cAPK (*28*), and a weak tail that extends as far as 95 Å. (In comparing MLCK and cAPK, it should be remembered that the latter structure does not have the equivalent 32 N-terminal residues and 57 C-terminal regulatory and CaM-binding residues of our MLCK construct.) The $P(r)$ function calculated from the basic scattering function of CaM-activated MLCK in the absence of substrates displayed a more compact structure than the uncomplexed kinase (Figure 3B). The tail observed for the uncomplexed MLCK is no longer present and the peak shifts to a lower r value (by ∼3 Å). The values for the R_g and d_{max} are also smaller for the complexed versus uncomplexed MLCK by 2.6 ± 2.0 Å and 17 Å, respectively [as reported by Krueger et al. (*1*)]. The

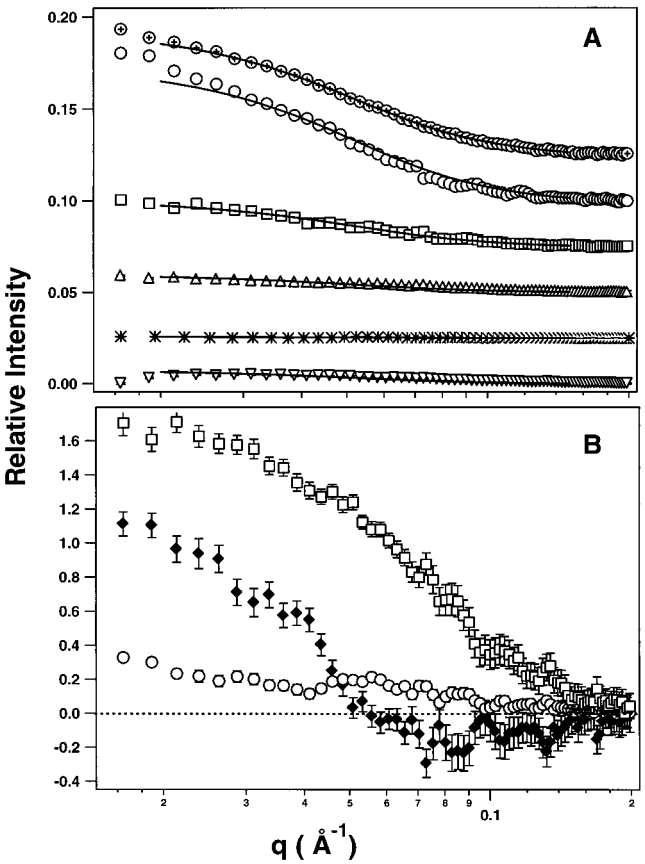

FIGURE 2: Scattering data for CaM·MLCK·pRLC·AMPPNP reduced to $I(Q)$ vs Q from X-ray scattering measurements (⊕), and neutron scattering measurements for samples in 0% (○), 20% (□), 40% (∗), 75% (△) and 85% (▽) D_2O. The scaling of the neutron-scattering data reflects their relative contrast factors, while the X-ray-scattering data are shown with an arbitrary scale relative to the neutron data for convenient presentation. Solid lines overlaying each data set represent $I(Q)$ vs Q calculated for a typical two-ellipsoid best-fit model to the data from $Q = 0.02$ to 0.15. (B) The basic scattering functions for MLCK plus substrates $I_K(Q)$ (□), for CaM $I_C(Q)$ (○) and for the cross-term $I_{CK}(Q)$ (◆) derived from the neutron and X-ray-scattering data.

observed changes in R_g and d_{max} for MLCK upon CaM binding are due mostly to a loss of the observed tailing of the $P(r)$ for uncomplexed MLCK. This tailing might be attributed to a very small degree of aggregation in the MLCK that is below the limits of uncertainty in the I_0 analysis. Alternatively, the N-terminus of MLCK may be extended in the uncomplexed MLCK. Our MLCK construct is truncated at the N-terminus and, therefore, may be missing

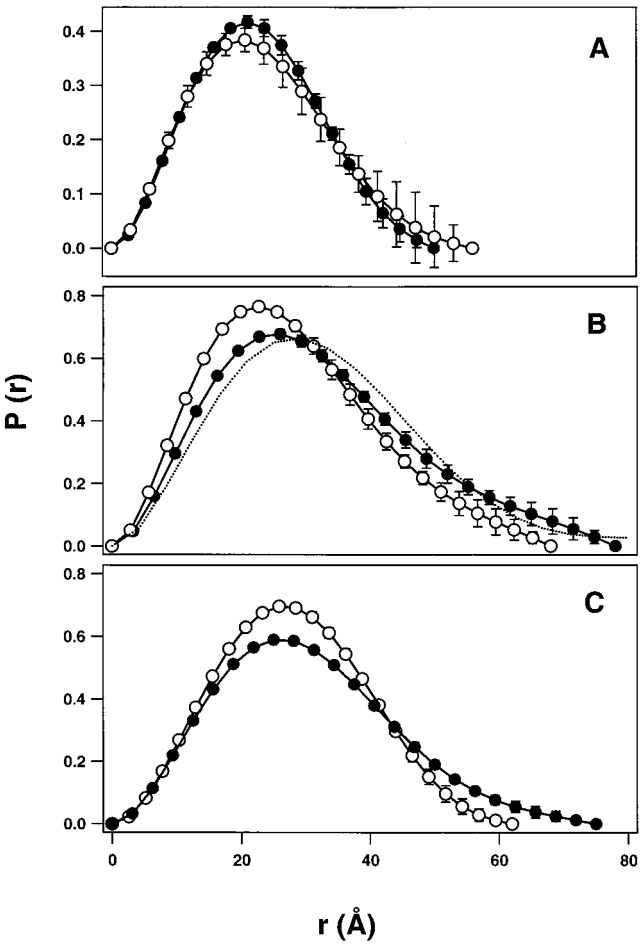

FIGURE 3: *P*(*r*) functions for (A) CaM and (B) MLCK from the basic scattering functions determined from the neutron contrast series data from CaM·MLCK (●) and CaM·MLCK·pRLC·AMPPNP (○). Also included in panel B is the *P*(*r*) determined for unactivated MLCK (···), without the full "tail" which continues at the same intensity out to ∼95 Å, from small-angle X-ray measurements taken at SSRL (*1*). (C) *P*(*r*) functions for cAMP-dependent protein kinase with (○) and without (●) bound protein kinase inhibitor peptide, PKI (*5*−*22*) (*28*) are included for direct comparison to panel B.

contacts with the rest of the protein important for stabilizing that part of the structure. In any case, the tailing, and thus its cause, is eliminated by CaM binding. The *P*(*r*) function calculated from the basic scattering function of CaM-activated MLCK in the presence of its substrates (Figure 3B) displays an even more compact structure than that without substrate present. The peak shifts to an even lower *r* value (by ∼3 Å), and the R_g and d_{max} values are smaller by 2.7 ± 1.1 Å and ∼10 Å, respectively (Table 1). Previously reported small-angle scattering measurements for cAPK detected reductions in R_g and d_{max} of 2 ± 0.8 Å and 11 Å, respectively, upon the binding of a peptide pseudosubstrate, the protein kinase inhibitor peptide PKIα(5−22)-amide (*28*; Figure 3C). More recent X-ray experiments on the catalytic subunit of cAPK in higher salt concentrations have shown that there can also be a peak shift of ∼2−3 Å to lower *r* values (*24*). This observed structural compaction has been accounted for by a closure of the catalytic cleft that sits between the small and large lobes of cAPK. The closure is achieved via a simple rotation about a hinge defined by a pair of glycine residues that are conserved throughout the

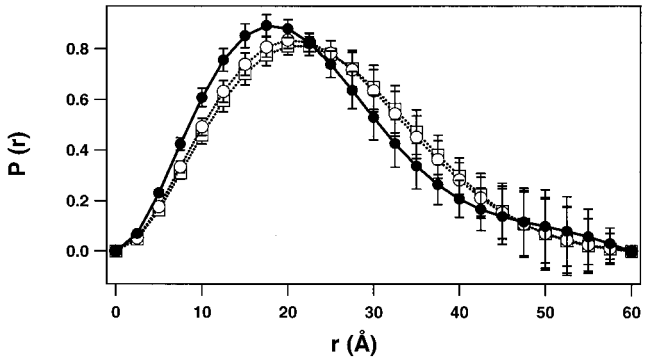

FIGURE 4: *P*(*r*) functions for CaM·MLCK·pRLC·AMPPNP (●), CaM·MLCK·AMPPNP (□) and for CaM·MLCK·pRLC (○) for neutron-scattering data collected in 82% D_2O buffer in which the deuterated CaM component is solvent matched.

CaM-dependent kinase family (*28*). The observed changes in R_g, d_{max} and the position of the peak in the *P*(*r*) for MLCK within the CaM·MLCK·pRLC·AMPPNP complex versus that for MLCK within the complex without substrates are each of the same magnitude and in the same direction as those observed for the closure of the catalytic cleft in cAPK. This comparison suggests that we also are observing closure of the catalytic cleft within the MLCK catalytic core upon substrate binding.

Solvent Matching of 62dCaM within the CaM•MLCK Complexes with AMPPNP and/or pRLC. Further evidence that we are observing a closure of the cleft between the two lobes of the MLCK catalytic core upon substrate binding comes from comparison of the *P*(*r*)s derived from small-angle neutron scattering data on the CaM·MLCK complex in the presence of AMPPNP, pRLC, or both of these substrates at 82% D_2O (Figure 4). The scattering density of the 62% deuterated CaM is very close to that of 82% D_2O, i.e., the 62dCaM is "solvent matched" and hence does not contribute significantly to the scattering. The *P*(*r*) curve obtained from the scattering data measured under these conditions therefore is dominated by vector lengths from the MLCK and substrates. The *P*(*r*) profiles calculated from these data are identical for the complex with either the AMPPNP or the peptide, however when both substrates are present, there is a measurable peak shift (∼3 Å) of the maximum in the *P*(*r*) to shorter vector lengths, and a reduction in the intensity of the vector lengths greater than 20 Å, characteristic of the catalytic cleft closure. Because these *P*(*r*) functions are calculated from a single contrast matching experiment, the counting statistics give rise to large errors. However, each measurement was done under identical conditions with the same neutron beam configuration, sample cells, and buffers in order to minimize systematic errors. Importantly, the same protein preparations were used to make each sample. The systematic shift in vector lengths observed only when both substrates are present is therefore significant, indicating that both AMPPNP and pRLC are required to see cleft closure in the kinase.

Modeling the Complex. Uniform-density, two-ellipsoid models for the CaM·MLCK·pRLC·AMPPNP complex were used to aid in the interpretation of the scattering data. Out of 5000 models generated, eight fit the constraints of predicting all of the scattering data giving a total $\chi < 1.6$ (see Figure 2A). Each of the final best-fit models were very

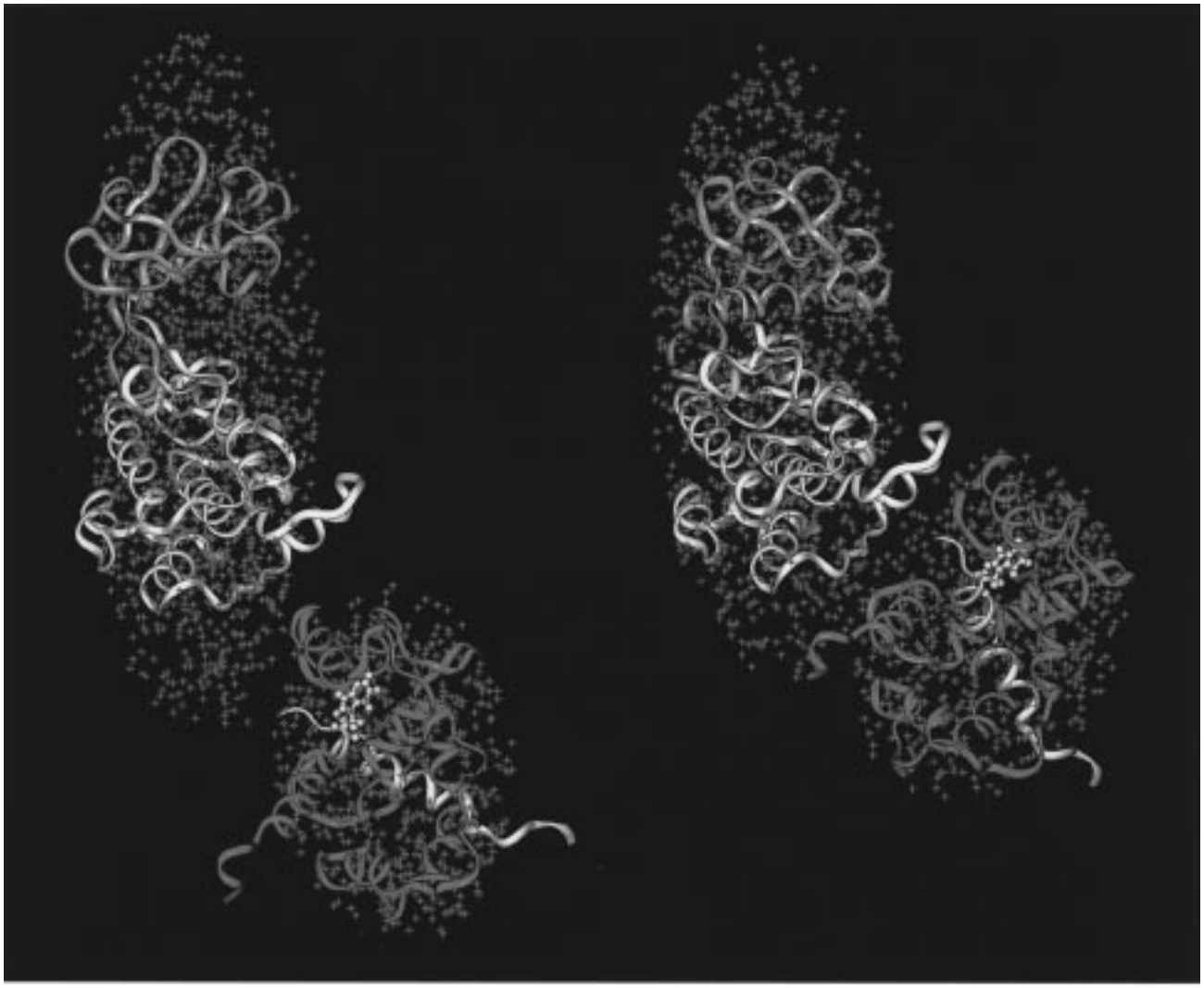

FIGURE 5: Models for the CaM/MLCK complexes with and without substrates. The green crosses represent the uniform density two-ellipsoid best-fit models to all of the scattering data for CaM·MLCK (left) and for CaM·MLCK·pRLC·AMPPNP (right). The average separation of the centers-of-mass of the CaM and MLCK components is 57.4 ± 1.8 and 45.2 ± 0.7, without and with substrates, respectively. The average ellipsoid semi-axes in angstroms are (44.6 ± 0.9, 23.9 ± 0.6, and 16.5 ± 0.5) for the larger MLCK ellipsoid and (24.7 ± 0.3, 23.1 ± 0.2, and 14.4 ± 0.1) for the smaller CaM ellipsoid in the complex without substrates (left). In the presence of substrates (right), the corresponding ellipsoid semi-axes are (41.3 ± 0.3, 24.0 ± 0.4, and 16.4 ± 0.1) and (26.4 ± 0.5, 22.4 ± 0.5, and 16.5 ± 1.0), respectively. Fit within the large ellipsoid from the CaM·MLCK (left) model is a ribbon representation (yellow with orange distinguishing the smaller N-terminal lobe) of the "open" conformation for the conserved catalytic core for all protein kinases based on the crystal structure of cAPK (*29*) and the solution scattering results of Olah et al. (*28*). Fit within the large ellipsoid from the CaM·MLCK·pRLC·AMPPNP (right) model is the conserved catalytic core structure of the inhibited cAPK crystal structure (yellow and orange ribbons; PDB no. 2cpk, residues 37−297). The NMR structure (PDB no. 2bbm) of CaM (red ribbon) complexed with MLCK−I (yellow ribbon with ball-and-stick representation of the N-terminal Trp) is fit within the smaller ellipsoids of both models. It is important to note that our scattering data leave some ambiguity with respect to the orientation of the catalytic cleft with respect to the CaM/MLCK interaction site (see text).

similar, having the same position of the smaller ellipsoid with respect to the larger one and exhibiting only minor differences in their relative twists. The separation of the centers of mass (D_{com}) for all the best-fit models is 45.2 ± 0.7 Å. The following two mathematical theories were also utilized for estimating D_{com} for CaM and MLCK from our neutron-scattering data on the CaM·MLCK·pRLC·AMPPNP complex: (1) calculation of the first moment of the Fourier transform of the cross-term [$I_{CK}(Q)$] gave a D_{com} of 58 ± 16 Å; and (2) analysis of the R_g as a function of contrast using the parallel axis theorem for a two-component system (*23*) gave a D_{com} of 49 ± 10 Å. All of the methods used to calculate D_{com} agree within error. However, the most reliable method for determining D_{com} comes from the modeling as this method is the only one which uses all of the scattering data.

SASMODEL also was used to find the best-fit two-ellipsoid model with respect to the previously published scattering data for the CaM·MLCK without substrates. The average ellipsoid dimensions (Figure 5 caption) and D_{com} value of 57.4 ± 1.8 Å is in excellent agreement with our previously published values which were obtained using a very similar modeling approach (*1*). Thus, upon substrate binding, we observe a decrease in D_{com} of 12.2 ± 2.5 Å. Figure 5 shows the two-ellipsoid models for the CaM·MLCK complex with and without bound substrates obtained using SASMODEL. These models show the compaction of MLCK within the complex upon substrate binding as a

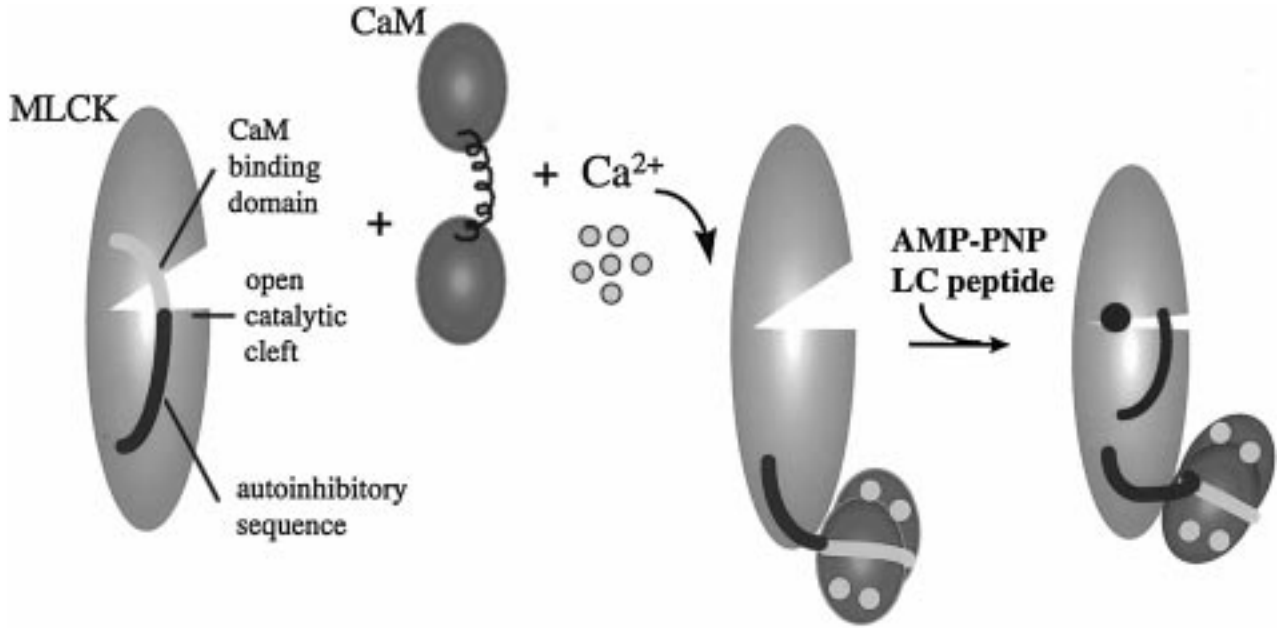

FIGURE 6: Schematic summarizing the sequential conformational transitions for CaM activation of MLCK as evidenced by our scattering results. In its inactive conformation, MLCK maintains an open catalytic cleft via numerous contacts with its regulatory segment. Upon binding Ca^{2+}, the hydrophobic clefts in each globular lobe of CaM are exposed. CaM then binds to the CaM-binding sequence of MLCK, undergoing an unhindered conformational collapse as it interacts with hydrophobic residues at each end of the CaM-binding sequence that forms a helix. MLCK autoinhibition is relieved as this binding induces a significant movement of the MLCK regulatory segment away from the surface of the catalytic core. Once CaM releases the autoinhibition of MLCK, substrate binding induces closure of the kinase catalytic cleft as well as a movement of the CaM center-of-mass toward that of MLCK. At the same time CaM reorients with respect to the kinase so as to bring about a close interaction between the N-terminal leader sequence of CaM and the kinase. Thus, the fully activated complex is formed.

shortening of the longest ellipsoid dimension for the kinase by ~7 Å, as well as a movement of the MLCK and CaM centers-of-mass toward each other.

High-resolution structures were each fit into the ellipsoids generated in the modeling studies (Figure 5). Specifically, we used the conserved portion of the catalytic core for all kinases based on the known crystal structure for inhibited cAPK with bound pseudosubstrate [PDB no. 2cpk, residues 37−297 (*29*)], a model of this structure with an "open" catalytic cleft (*28*), and the NMR structure of CaM bound to MLCK−I peptide (*13*). The open catalytic core structure was fit into the ellipsoid representing the kinase without substrates and the inhibited (closed) catalytic core structure was fit into the ellipsoid representing the kinase with substrates bound. Both of these structures are missing the 32 N-terminal residues and 29 C-terminal residues extending from the C-terminus of the catalytic core to the beginning of the CaM-binding domain (MLCK−I). The empty volumes at the top and bottom of each of the kinase ellipsoids are expected to be occupied by these residues. As was the case for the previously published CaM·MLCK structure (*1*), the asymmetry in the ellipsoid dimensions (Figure 5 caption) for the high-resolution structures of each component is well reflected in the ellipsoid models. The CaM structure was placed within its respective ellipsoids so as to place the N-terminus of the MLCK−I peptide toward the kinase such that it can connect with the inhibitory sequence of the MLCK. The combination of this connectivity requirement and the asymmetry of the CaM ellipsoid shape (average ellipsoid dimensions of 25.5, 22.7, and 15.5 Å) fairly well constrains the orientation of CaM with respect to the kinase ellipsoid. An intriguing observation stemming from these fits is that the model of the complex with substrates shows a reorientation of the CaM with respect to the kinase such that the N-terminal sequence of CaM makes contact with the MLCK. In contrast, for the complex without substrates, CaM could not be fit within its ellipsoid such that the N-terminus of CaM interacts with MLCK and at the same time have the N-terminus of MLCK−I connect with the kinase. This constraint results from the orientation of the long axis of the CaM structure with respect to that of the kinase. In the complex without substrates, these axes are almost parallel (in the plane of Figure 5), whereas they are at a significant angle in the complex with substrates. This reorientation of CaM upon substrate binding is intriguing considering the results of Persechini et al. (*30*). They observed that deletion of the N-terminal leader sequence of CaM (residues 2−8) abolishes CaM-dependent activation of skeletal muscle MLCK, and reduces the CaM-dependent activation of smooth muscle MLCK by 50%, but has no effect of the apparent affinities of CaM for either MLCK. They further were able to show that it was the acidic cluster Glu^6-Glu^7-Gln^8 that contains the critical determinants for activation. These data were somewhat surprising, because the N-terminal leader sequence appears to have little or no structural role evident in the high-resolution structures of CaM (*9*) or of its complexes with the CaM-binding peptides derived from either smooth or skeletal muscle MLCK (*13*, *14*). Persechini and colleagues proposed that the acidic Glu^6-Glu^7-Gln^8 cluster in the N-terminal leader sequence of CaM interacts with one or more basic residues that flank the CaM-binding domain in MLCK and that these interactions are important in activation but not for binding. Our scattering results support this proposal.

It is important to note with respect to Figure 5 that there is some ambiguity with regard to the orientation of the

catalytic cleft with respect to the CaM/MLCK interaction site. Because of the 2-fold symmetry of the kinase ellipsoid, it is possible to rotate the catalytic core structure 180° about its long axis, thus orienting the catalytic site such that it opens in the opposite direction with respect to the CaM/MLCK interaction site. There are two additional 2-fold axes perpendicular to each other and to the long axis of the kinase ellipsoid. A 180° rotation of the catalytic core about either of these axes would invert the structure so as to place the small lobe at the bottom of the kinase ellipsoid and nearest the CaM/MLCK interface (Figure 5). We have previously argued that the orientation shown in Figure 5 with the small lobe of the catalytic core at the top is the one that is most reasonable because it easily allows for the required connectivity between the autoinhibitory and CaM-binding sequences of MLCK.

Implications of the Scattering Results for the Activation Mechanism. Figure 6 summarizes what we have learned about the activation of MLCK by CaM from our solution-scattering experiments described in this paper and in our previous work on the complex without substrates (*1*). Previous studies have shown that, in its auto-inhibited conformation, the catalytic core of MLCK maintains inhibition via numerous contacts with its regulatory segment, which includes both an autoinhibitory sequence as well as the CaM-binding domain (*6*−*8*). Our previous neutron-scattering study has shown that, upon binding MLCK, CaM undergoes an unhindered conformational collapse (*1*) and releases autoinhibiton of the kinase by inducing a significant movement of its regulatory segment away from the surface of the catalytic core. Our current neutron-scattering study supports the conclusion that, once inhibition is released by CaM, the kinase can bind and close about its substrates in order to bring together the chemical constituents required for catalysis. Both MLCK substrates, the phosphorylation sequence for myosin regulatory light chain and ATP, are required for closure. Accompanying closure of the catalytic cleft within the MLCK is a movement of the CaM and MLCK centers-of-mass toward each other, and a reorientation of CaM so that its N-terminal sequence interacts with the kinase surface. Neutron scattering and contrast variation have thus allowed us to follow sequentially the conformational transitions in the CaM-dependent activation of MLCK in solution, yielding important structural data that defines the mechanistic steps in the release of autoinhibiton of MLCK by CaM, as well as subsequent substrate binding and activation.

ACKNOWLEDGMENT

We wish to thank Nicholas A. Bishop for technical assistance in the neutron data acquisition and reduction and Sue Rokop for preparation of the deuterated CaM. We thank Griselda Hernández for the NMR data used to calculate the deuteration levels in CaM. We thank Drs. Susan Krueger and Charles Glinka for assistance in the neutron scattering data acquisition at NIST and Dr. H. Tsuruta for assistance in X-ray scattering data acquisition at SSRL.

REFERENCES

1. Krueger, J. K., Olah, G. A., Rokop, S. E., Zhi, G., Stull, J. T., and Trewhella, J. (1997) *Biochemistry 36*, 6017−6023.
2. Stull, J. T. (1988) in *Molecular Aspects of Cellular Regulation* (Cohen, P., and Klee, B. C., Eds.) Vol. 5, pp 91−119, Elsevier, Amsterdam.
3. Stull, J. T., Krueger, J. K., Kamm, K. E., Gao, Z.-H., Zhi, G., and Padre, R. (1996) in *Biochemistry of Smooth Muscle Contraction* (Barany, M., Ed.) pp 119−128, Academic Press, Inc., San Diego.
4. Kemp, B. E., Parker, M. W., Hu, S. H., Tiganis, T., and House, C. (1994) *Trends Biochem. Sci. 19*, 440−444.
5. Stull, J. T., Krueger, J. K., Zhi, G., and Gao, Z.-H. (1995) In *International Symposium on Regulation of the Contractile Cycle in Smooth Muscle*, MIE, Japan.
6. Krueger, J. K., Padre, R. C., and Stull, J. T. (1995) *J. Biol. Chem. 270*, 16848−16853.
7. Gallagher, P. J., Herring, B. P., Trafny, A., Sowadski, J., and Stull, J. T. (1993) *J. Biol. Chem. 268*, 26578−26582.
8. Kemp, B. E., and Pearson, R. B. (1991) *Biochim. Biophys. Acta 1094*, 67−76.
9. Babu, Y. S., Bugg, C. E., and Cook, W. J. (1988) *J. Mol. Biol. 204*, 191−204.
10. Clore, G. M., Bax, A., Ikura, M., and Gronenborn, A. M. (1993) *Curr. Opin. Struct. Biol. 3*, 838−845.
11. Ikura, M. (1996) *Trends Biochem. Sci. 21*, 14−17.
12. Heidorn, D. B., Seeger, P. A., Rokop, S. E., Blumenthal, D. K., Means, A. R., Crespi, H., and Trewhella, J. (1989) *Biochemistry 28*, 6757−6764.
13. Ikura, M., Clore, G. M., Gronenborn, A. M., Zhu, G., Klee, C. B., and Bax, A. (1992) *Science 256*, 632−638.
14. Meador, W. E., Means, A. R., and Quiocho, F. A. (1992) *Science 257*, 1251−1255.
15. Gao, Z.-H., Zhi, G., Herring, B. P., Moomaw, C., Deogny, L., Slaughter, C. A., and Stull, J. T. (1995) *J. Biol. Chem. 270*, 10125−10135.
16. Olah, G. A., Rokop, S. E., Wang, A. C. -L, Blechner, S. L., and Trewhella, J. (1994) *Biochemistry 33*, 8233−8239.
17. Michnoff, C. H., Kemp, B. E., and Stull, J. T. (1986) *J. Biol. Chem. 261*, 8320−8326.
18. Kringbaum, W. R., and Kugler, F. R. (1970) *Biochemistry 9*, 1216.
19. Wakatsuki, S., Hodgson, K. O., Eliezer, D., Rice, M., Hubbard, S., Gillis N., Donniach, S., and Spann, U. (1992) *Rev. Sci. Instrum. 63*, 1736−1740.
20. Heidorn, D. B., and Trewhella, J. (1988) *Biochemistry 27*, 909−915.
21. Hammouda, B., Barker, J. G., and Krueger, S. (1996) *Small-Angle Neutron Scattering Manuals* (NIST), Gaithersburg, MD.
22. Ibel, K., and Stuhrmann, H. B. (1975) *J. Mol. Biol. 93*, 255−265.
23. Moore, P. B. (1981) *J. Appl. Crystallogr. 14*, 237−240.
24. Zhao, J, Hoyer, E., Boylen, S., Walsh, D. A., and Trewhella, J. (1998) *J. Biol. Chem.* (submitted for publication).
25. Porod, G. (1982) *Small-Angle X-ray Scattering*, pp 17−51, Academic Press, New York.
26. Stuhrmann, H. B. (1987) *Methods of Experimental Physics*, pp 367−403, Academic Press, Inc., New York.
27. Moore, P. B. (1980) *J. Appl. Crystallogr. 13*, 168−175.
28. Olah, G. A., Mitchell, R. D., Sosnick, T. R., Walsh, D. A., and Trewhella, J. (1993) *Biochemistry 32*, 3649−3657.
29. Knighton, D. R., Zheng, J. H., Ten Eyck, L. F., Ashford, V. A., Xuong, N. H., Taylor, S. S., and Sowadski J. M. (1991) *Science 253*, 407−414.
30. Persechini, A., Gansz, K. J., and Paresi, R. J. (1996) *J. Biol. Chem. 271*, 19279−19282.

BI981311D